Supplementary Information

Testing tree crown economics with National Ecological Observatory Network

Yiting Fan[1,3,*], Andrew J. Elmore[2] & Brenden E. McNeil[1]

[1] Department of Geology and Geography, West Virginia University, Morgantown, WV, USA

[2] University of Maryland Center for Environmental Science, Appalachian Laboratory, Frostburg, MD, USA

[3] Present address: Department of Environmental Sciences, University of Virginia, Charlottesville, VA, USA

* Corresponding author: ricycastillo@gmail.com

Supplementary Figure S1

3-D Tree Crown Extraction methods

Prior to extracting the crown traits from the NEON AOP LiDAR data, we conducted several steps of data cleaning and filtering to obtain high-quality tree crown architecture data. To avoid potential confounding effects from unknown objects such as birds, we removed points exceeding 99% outer canopy height. To ameliorate poor data quality caused by other issues such as image mis-alignment, we then selected the field-delineated tree crowns that met four criteria. First, we excluded crowns with extremely sparse point cloud density, defined as: (1) point spacing leading to large gaps between points (more than 10 centimeters); (2) fewer than 10 points/m^3 on average; or (3) inadequate crown coverage. Sparse point clouds in these crowns were likely caused by dense foliage and canopy overlap leading to severe laser occlusion. Second, we checked the delineation for each crown using the 0.1m-resolution orthorectified images captured by the AOP platform (Figure S1). From this visual check, we discarded crowns with delineations that clearly included neighboring crowns or that primarily covered canopy gaps. Third, to remove returns from the understory or sub-canopy trees, we eliminated point clouds below a site-specific crown base height. We defined crown base height for each site using a vertical profile of photosynthetically active radiation (PAR) collected at multiple heights on each tower (NEON DP1.00024.0). Based on the PAR vertical profile, we set the base height for each site to the lower threshold point where the tangent line of the curve approaches vertical (Figure S1). The resulting base heights for each site are reflected in Table 1 of the main paper. Finally, we ensured that the vertical profiles of LiDAR intensity (defined as the returned signal strength, which depends on surface reflectance, sensor properties, and atmospheric conditions) and plant area density (PAD) were in reasonable alignment with vertical PAR profiles, which attenuate with height (Figure S1). Likely due to the presence of overtopped understory trees whose crowns overlapped with a delineated canopy tree, we eliminated crowns that markedly deviated from the expected pattern of PAD decreasing as PAR decreased from the top of the crown. Out of 305 total crowns delineated by NEON at the nine sites, we removed 7 crowns due to one or more of these quality controls.

We computed PAI as the column sum of PAD (Almeida et al., 2019; Kamoske et al., 2019), defined as the ratio of LiDAR plant returns to all pulses within each 1-m^3 voxel in each vertical column (Kamoske et al., 2019). We used R_t to describe the variability of the outer crown surface, computed as the standard deviation of column maximum height within each crown (Atkins et al., 2018). We calculated $APAD_{50}$ as the proportion of PAD occurring above the midpoint of the crown, determined from each crown's maximum height and site-specific crown base height (yellow dot and red dash lines in Figure S1). To ensure methodological consistency and maintain trait independence, we applied a fixed light extinction coefficient (k) of 0.5 across all sites, despite known variation due to factors like leaf angle distribution (Zhang et al., 2014). Trait calculations used the lidR (Roussel et al., 2020), canopylazR (Kamoske et al., 2019), and leafR (Almeida et al., 2019) R packages.

Figure S1: Example visualization of the 3D point-cloud extraction procedures for a Liriodendron tulipifera tree at the ORNL site. For each field-delineated crown (shown on the inset AOP high resolution photo), we used the crown specific vertical profiles of LiDAR intensity and PAD, as well as the site-specific PAR data to quality check candidate crowns and determine the crown base height. The red lines denote the crown top, site-specific crown base height and the middle point (50%).

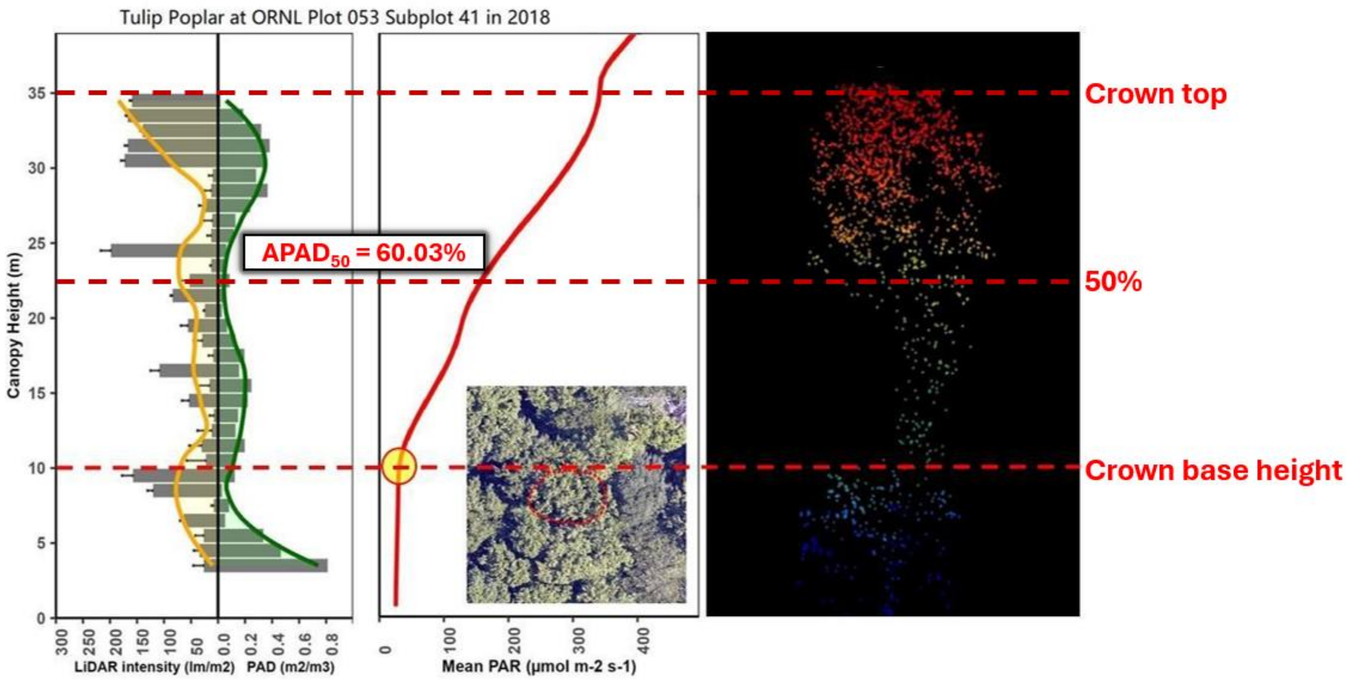

Supplementary Figure S2

Comparison between NEON directional- and bidirectional-derived NIR_v

During our study period, NEON upgraded the pre-processing workflow of the AOP imaging spectrometer data that we used to derive NIR_v values, with imagery from 2022 and forward processed using an improved algorithm to account for bidirectional reflectance. However, to align AOP image dates with available quality leaf angle data that we measured from NEON towers, we needed to use the earlier directional reflectance imagery for five out of the nine sites (see Table 1 in the main text for leaf angle and AOP image dates). To test for any systematic bias among the two algorithms, we were able to compare NIR_v data obtained in 2021 with the directional algorithm versus NIR_v data obtained in 2022 with the bidirectional algorithm (Figure S2). Across and within sites, crown-level NIR_v values from the two years were highly correlated, with regression slopes close to 1 and small intercepts, indicating no strong systematic bias between the products. The systematic bias was likely minimal because of within-crown pixel averaging, and the nature of NIRv as a ratio. While generally small relative to the large spatial variability, residual differences among the 2021 and 2022 data were likely attributable to a combination of factors, including differences in data acquisition conditions (e.g., sun/sensor/target geometry, atmospheric conditions), and inter-annual differences in phenological timing.

Figure S2 Comparison of crown-scale NIR_v from the 2021 directional and 2022 bidirectional NEON products at GRSM, SCBI, and SERC, as demonstrated by adjusted R^2, F-statistics and significances. Points are colored by sites. Black line represents identity line and green line represents regression line. The 2022 AOP acquisitions at these sites occurred on [GRSM: 05/20/2022; 09/23/2022; 09/27/2022 - 09/29/2022], [SCBI: 05/30/2022], and [SERC: 05/29/2022; 05/30/2022]. The 2021 dates are provided in Table 1 of the main text.

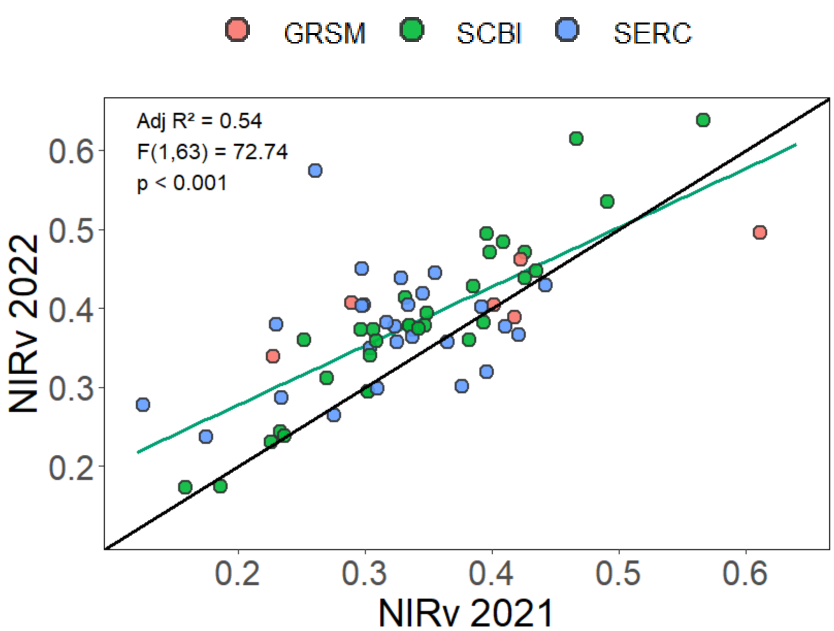

Supplementary Table S1

Leave-one-out sensitivity analysis for the MLA-$APAD_{50}$, MLA-NIR_v, and $APAD_{50}$-NIR_v relationships

Table S1: Results of leave-one-out sensitivity analyses for the three key bivariate relationships ($APAD_{50}$-NIR_v, MLA-$APAD_{50}$, and MLA-NIR_v) shown in Figure 2. Each model was refit 13 times, with one site-species combination removed at a time. The table is grouped by relationship and, within each relationship, sorted in descending order by adjusted R^2.

Omitted site	Omitted species	Relationship	Adjusted R^2	F	p-value
ORNL	*Quercus montana*	APAD50–NIRv	0.330	6.310	0.031
UNDE	*Acer saccharum*	APAD50–NIRv	0.130	2.710	0.130
BART	*Acer rubrum*	APAD50–NIRv	0.130	2.620	0.137
UKFS	*Carya ovata*	APAD50–NIRv	0.120	2.470	0.147
ORNL	*Liriodendron tulipifera*	APAD50–NIRv	0.120	2.570	0.140
MLBS	*Acer rubrum*	APAD50–NIRv	0.100	2.200	0.169
ORNL	*Quercus velutina*	APAD50–NIRv	0.090	2.140	0.174
BART	*Betula alleghaniensis*	APAD50–NIRv	0.090	2.110	0.177
GRSM	*Liriodendron tulipifera*	APAD50–NIRv	0.080	1.910	0.197
SERC	*Liriodendron tulipifera*	APAD50–NIRv	0.050	1.580	0.237
SERC	*Carya ovata*	APAD50–NIRv	0.040	1.450	0.256
SCBI	*Liriodendron tulipifera*	APAD50–NIRv	0.040	1.490	0.250
TREE	*Acer saccharum*	APAD50–NIRv	0.030	1.350	0.273
UNDE	*Acer saccharum*	MLA–APAD50	0.460	10.330	0.009
SERC	*Carya ovata*	MLA–APAD50	0.380	7.660	0.020
ORNL	*Quercus montana*	MLA–APAD50	0.370	7.460	0.021
ORNL	*Liriodendron tulipifera*	MLA–APAD50	0.350	6.990	0.025
MLBS	*Acer rubrum*	MLA–APAD50	0.340	6.600	0.028
GRSM	*Liriodendron tulipifera*	MLA–APAD50	0.320	6.130	0.033
UKFS	*Carya ovata*	MLA–APAD50	0.310	5.990	0.034
BART	*Betula alleghaniensis*	MLA–APAD50	0.300	5.800	0.037
SERC	*Liriodendron tulipifera*	MLA–APAD50	0.270	5.060	0.048
TREE	*Acer saccharum*	MLA–APAD50	0.270	5.020	0.049
BART	*Acer rubrum*	MLA–APAD50	0.260	4.920	0.051
ORNL	*Quercus velutina*	MLA–APAD50	0.250	4.600	0.058
SCBI	*Liriodendron tulipifera*	MLA–APAD50	0.180	3.480	0.092
UKFS	*Carya ovata*	MLA–NIRv	0.520	12.780	0.005
ORNL	*Quercus montana*	MLA–NIRv	0.460	10.280	0.009
SERC	*Carya ovata*	MLA–NIRv	0.450	10.000	0.010
ORNL	*Quercus velutina*	MLA–NIRv	0.450	9.910	0.010
BART	*Acer rubrum*	MLA–NIRv	0.440	9.770	0.011
GRSM	*Liriodendron tulipifera*	MLA–NIRv	0.410	8.510	0.015
ORNL	*Liriodendron tulipifera*	MLA–NIRv	0.400	8.230	0.017
MLBS	*Acer rubrum*	MLA–NIRv	0.380	7.680	0.020
SCBI	*Liriodendron tulipifera*	MLA–NIRv	0.370	7.370	0.022
TREE	*Acer saccharum*	MLA–NIRv	0.370	7.360	0.022
SERC	*Liriodendron tulipifera*	MLA–NIRv	0.360	7.310	0.022
BART	*Betula alleghaniensis*	MLA–NIRv	0.340	6.720	0.027
UNDE	*Acer saccharum*	MLA–NIRv	0.310	6.000	0.034

Supplementary Table S2

Dataset of the 13 site–species combinations used in the cross-site analyses. Values are means and associated standard errors (se) unless otherwise indicated.

Species	AOP.year	Site	n_ crown	PAI	se_ PAI	Rt	se_Rt	MAXCH	se_ MAXCH	APAD50	se_ APAD50	NIRv	se_ NIRv	MLA	se_ MLA	Moisture Index	VPD	Temp	RH
Carya ovata	2022	UKFS	5	8.74	0.53	4.98	0.89	19.23	0.91	57.56	1.77	0.42	0.01	41.40	1.35	0.68	-	-	-
Liriodendron tulipifera	2021	SERC	2	10.10	1.70	6.27	0.18	33.38	0.93	64.51	4.52	0.32	0.01	41.86	1.15	0.81	0.55	23.26	80.48
Carya ovata	2021	SERC	4	9.72	2.24	5.22	0.57	29.54	0.58	66.72	2.85	0.32	0.04	35.77	1.12	0.81	0.55	23.26	80.48
Liriodendron tulipifera	2021	SCBI	5	6.74	0.92	7.46	1.07	30.62	2.26	70.44	4.71	0.33	0.01	46.05	1.28	0.85	1.03	24.94	69.38
Acer saccharum	2022	TREE	3	8.03	1.49	6.95	1.08	21.20	1.76	38.83	10.73	0.44	0.01	29.75	1.13	0.88	-	-	-
Acer rubrum	2021	MLBS	4	9.29	0.80	4.77	0.29	20.53	0.67	56.55	6.60	0.34	0.02	43.32	0.86	0.91	0.63	20.33	73.63
Quercus velutina	2018	ORNL	2	9.26	0.41	7.57	2.55	33.18	4.80	46.05	4.42	0.40	0.00	26.20	1.69	0.95	0.40	22.73	85.13
Quercus montana	2018	ORNL	4	8.55	0.98	5.60	1.20	29.10	0.97	60.27	1.56	0.50	0.02	32.06	1.29	0.95	0.40	22.73	85.13
Liriodendron tulipifera	2018	ORNL	4	10.43	0.92	6.01	1.66	31.60	1.02	49.82	6.07	0.36	0.01	38.21	1.35	0.95	0.40	22.73	85.13
Acer saccharum	2022	UNDE	5	8.85	1.53	3.13	0.82	19.93	1.44	55.82	12.26	0.46	0.03	24.18	1.48	0.96	0.64	19.99	72.40
Liriodendron tulipifera	2021	GRSM	2	4.71	1.96	4.62	0.21	25.23	5.71	48.19	8.74	0.42	0.00	34.70	0.88	1.20	0.38	22.64	85.65
Acer rubrum	2022	BART	4	10.54	1.10	3.91	0.89	24.05	1.23	44.62	1.53	0.38	0.03	29.65	1.24	1.31	-	-	-
Betula alleghaniensis	2022	BART	3	10.04	0.99	3.33	1.14	23.36	2.77	59.17	9.96	0.28	0.08	42.99	1.14	1.31	-	-	-

Supplementary References

1. Almeida, D. R. A. et al. Optimizing the remote detection of tropical rainforest structure with airborne lidar: leaf area profile sensitivity to pulse density and spatial sampling. Remote Sens. 11, 92; https://doi.org/10.3390/rs11010092 (2019).

2. Atkins, J. W. et al. Quantifying vegetation and canopy structural complexity from terrestrial LiDAR data using the forestr R package. Methods Ecol. Evol. 9, 2057–2066; https://doi.org/10.1111/2041-210X.13061 (2018).

3. Kamoske, A. G., Dahlin, K. M., Stark, S. C. & Serbin, S. P. Leaf area density from airborne LiDAR: comparing sensors and resolutions in a temperate broadleaf forest ecosystem. For. Ecol. Manage. 433, 364–375; https://doi.org/10.1016/j.foreco.2018.11.017 (2019).

4. Roussel, J.-R. et al. lidR: an R package for analysis of airborne laser scanning data. Remote Sens. Environ. 251, 112061; https://doi.org/10.1016/j.rse.2020.112061 (2020).

5. Zhang, L., Hu, Z., Fan, J., Zhou, D. & Tang, F. A meta-analysis of the canopy light extinction coefficient in terrestrial ecosystems. Front. Earth Sci. 8, 599–609; https://doi.org/10.1007/s11707-014-0446-7 (2014).